Calculations for electron-ion collisions and photoionization processes for plasma modelling

N R Badnell

Department of Physics, University of Strathclyde, Glasgow, G4 0NG, UK

Abstract. We discuss and illustrate our recent work on dielectronic recombination, photoionization & opacities, and electron-impact excitation, with a particular view to its application for plasma modelling.

1. Introduction

Dielectronic recombination (DR) is interesting in that it is the dominant electron–ion recombination process in both photoionized and electron-collisional plasmas. As such, it is necessary to have knowledge of DR over many orders of magnitude of temperature because the temperatures of peak and range of significant abundance of an ion differ greatly between the two types of plasma. (These occur at roughly $1/20^{\text{th}}$ of the ionization potential in the former case and $1/2$ in the latter.) The resonant states which contribute in the two temperature regimes are, thus, rather different. In the low-temperature photoionized plasmas typically only a few resonances near threshold survive the Maxwellian exponential cut-off. Of historical note, it was this low temperature regime (albeit in the Earth's upper atmosphere) for which DR was first considered, by Massey & Bates (1942–3). It was in this context that Bates' student Seaton (1962) first estimated the importance of DR in the solar corona, and so underestimated it. In turn, it was Seaton's student Burgess who in 1964 first demonstrated that high Rydberg states (and their associated high statistical weighting) become paramount in the high-temperature collisional plasmas.

In section 2 of this paper we look at some current problems in DR. In section 3 we look at the closely related problem of (the inverse process of) photoionization and its application to opacity determination, and some current problems of interest therein. Finally, in section 4, we look at some new developments for determination of R-matrix electron-impact excitation data for spectroscopic diagnostic plasma modelling.

2. Dielectronic recombination

We use the independent processes, isolated resonances using distorted waves (IPIRDW) approach to dielectronic recombination, as implemented within the AUTOSTRUCTURE code (Badnell, 1987). A detailed discussion of the validity of this approach is given by Pindzola *et al* (1992), while its advantages from a (collisional–radiative) modelling perspective is discussed by Badnell *et al* (2003).

2.1. The IPIRDW approach

In the IPIRDW approach, the partial dielectronic recombination rate coefficient $\alpha_{i\nu}^{z+1}$ from an initial metastable state ν of an ion X^{+z+1} into a resolved final state i of an ion X^{+z} is given by (Burgess, 1964)

$$\alpha_{i\nu}^{z+1} = \left(\frac{4\pi a_0^2 I_{\mathrm{H}}}{k_{\mathrm{B}} T_{\mathrm{e}}}\right)^{3/2} \sum_j \frac{\omega_j}{2\omega_\nu} \times \frac{\sum_l A_{j\to\nu,E_cl}^{\mathrm{a}} A_{j\to i}^{\mathrm{r}}}{\sum_h A_{j\to h}^{\mathrm{r}} + \sum_{m,l} A_{j\to m,E_cl}^{\mathrm{a}}} \, \mathrm{e}^{-E_c/(k_{\mathrm{B}} T_{\mathrm{e}})} \,, \qquad (1)$$

where ω_j is the statistical weight of the $(N+1)$-electron doubly-excited resonance state j, ω_ν is the statistical weight of the N-electron target state (so, $z = Z - N - 1$) and the autoionization (A^{a}) and radiative (A^{r}) rates are in inverse seconds. Here, E_{c} is the energy of the continuum electron (with orbital angular momentum l), which is fixed by the position of the resonances, and I_{H} is the ionization potential energy of the hydrogen atom (both in the same units of energy), k_{B} is the Boltzman constant, T_{e} the electron temperature and $(4\pi a_0^2)^{3/2} = 6.6011 \times 10^{-24}$ cm^3.

The effect of interacting resonances on dielectronic recombination has been investigated by Pindzola *et al* (1992) and can safely be neglected, as far as plasma modelling is concerned, at least in the absence of external electric and magnetic fields. Interference between DR and radiative recombination (RR) was also considered in detail by Pindzola *et al* (1992). The first-order effect (in $1/q$, where q is the Fano q-factor) arises as an asymmetry in the line-profile, as seen in high-resolution photoionization measurements. But, when averaged-over the resonance line-profile, it vanishes identically — see also Badnell & Pindzola (1992) and Behar *et al* (2000). So, it is the second-order effect ($1/q^2$) which is the leading correction to the Maxwell rate coefficient, and most merged-beams measurements of DR, and can safely be neglected for plasma modelling.

2.2. Application to the Fe M-shell problem

The iron M-shell ions (predominantly Fe^{7+} – Fe^{13+}) give rise to strong X-ray absorption lines due to $n = 2-3$ electronic inner-shell transitions. These are seen in the spectra of active galactic nuclei (AGNs) observed by *Chandra* and *XMM-Newton* (Sako *et al* , 2001) as an unresolved-transition-array (UTA). The shape of the UTA feature can be used as a powerful diagnostic of warm absorbers — see Behar *et al* (2001) for a detailed discussion. However, Netzer *et al* (2003) have pointed-out problems in modelling this shape and so Netzer (2004), using ION, and Kraemer *et al* (2004), using CLOUDY, have suggested increasing the magnitude of the recombination rate coefficients for Fe ions, particularly the $3p^q$ ($q = 1 - 6$) ions Fe^{13+} – Fe^{8+}, by postulating *ad hoc* low-temperature dielectronic recombination rate coefficients. The net effect is to shift the ionization balance towards the neutral end. This brings the modelling results towards accord with observation, but it is not rigorous since there is little to constrain the DR rate coefficients which they use.

The extant recombination data is effectively all radiative at photoionized plasma temperatures, as the recommended DR data for these Fe ions (Arnaud & Raymond, 1982) give essentially zero-contribution at photoionized plasma temperatures (being based on high temperature data for electron-collisional plasmas of Jacobs *et al* , 1977, and Hahn, 1985). There is much evidence from the Fe L-shell, both experimental and theoretical (see, e.g., Savin *et al* , 2006) that a significant contribution can be expected from DR at low temperatures, due principally to 'non-dipole' core-excitations.

We have carried-out AUTOSTRUCTURE calculations for Fe^{q+} (Badnell, 2006a,b) utilizing a target of the form: $3s^2 3p^q$, $3s 3p^{q+1}$, $3s^2 3p^{q-1} 3d$, $3p^{q+2}$, $3s 3p^q 3d$, $3s^2 3p^{q-2} 3d^2$, $3p^{q+1} 3d$. We show the results for Fe^{13+} ($q = 1$) in figure 1, where we make a number of comparisons. Firstly, the total DR rate coefficient is an order of magnitude larger than the RR one at photoionized plasma temperatures, indicating that the previous guesses at the low temperature DR values were considerably conservative. Secondly, there is good agreement with the previously
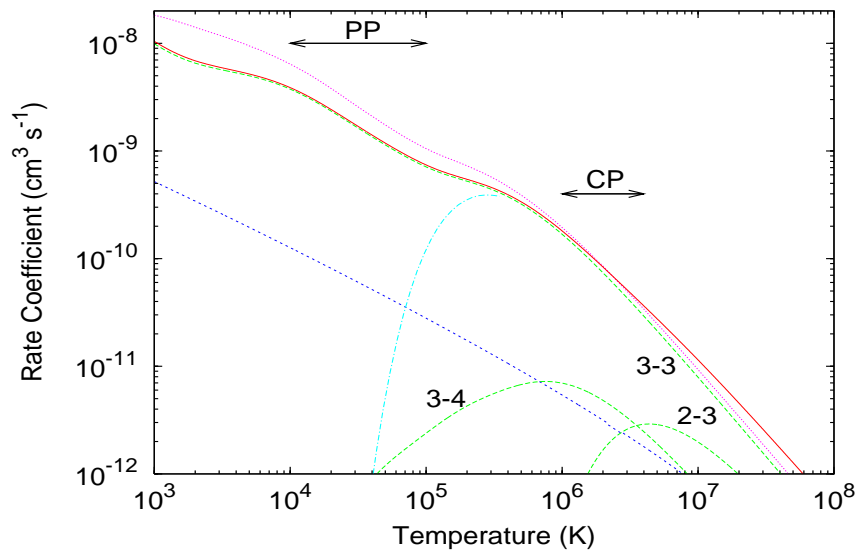
Figure 1. Maxwellian rate coefficients for Fe^{13+}. Solid (red) curve, total DR-plus-RR; short-dashed (blue) curve, RR; long-dashed (green) curves, DR for $3-3$, $3-4$ and $2-3$ core-excitations (Badnell, 2006a). Dot-dashed (light blue) curve, recommended DR of Arnaud & Raymond (1992). Dotted (purple) curve, experimentally based total of Schmidt *et al* (2006). PP and CP denote typical photoionized and electron-collisional plasma temperature ranges, respectively, for Fe^{13+} (Kallman & Bautista 2001, and Mazzotta *et al* 1998). (Colour online.)

recommended high temperature DR values of Arnaud & Raymond (1982). Thirdly, the DR rate coefficients determined by Schmidt *et al* (2006) from measurements of DR in an electron cooler at the heavy-ion storage ring at GSI, are somewhat larger still — by up to 50% down at 10^4 K. Finally, the relatively small contribution, as it turns out, from $\Delta n = 1$ core-excitations is also shown. This justifies their neglect for the remaining Fe ions ($q = 2 - 6$). The rest of the Fe $3p^q$ isonuclear sequence shows a similar trend of a DR contribution which is order magnitude larger than RR (and, so, the extant total) — see Badnell (2006b) for full details.

Further experimental measurements are in the course of being analysed and compared against theory, viz. Fe^{7-10+} (Schmidt, private communication, 2007). Clearly, other M-shell ions of importance to modelling photoionized plasmas need to be reconsidered, e.g., Sulphur. Lower-charge ions are problematical. Even Fe^{8+} represents the limit of where theory can reasonably position the low-lying resonances. Since the position of *identifiable* autoionizing energy levels, and associated resonances, are rarely known for the M-shell, their positioning is based upon a knowledge of target parent (bound) energy levels and the assumption that the captured 'Rydberg' electron interacts weakly with the core. By Fe^{7+}, the paucity of known target levels, and the fact that the low temperature DR is dominated by capture to $n = 4$, means that reasonably accurate theoretical low-temperature DR rate coefficients will be a challenge to produce here.

2.3. DR data for plasma modelling
We identify the differing DR requirements of different plasma regimes.

2.3.1. Coronal plasmas. This is the historic example, for which initial ground-state zero-density totals for (high temperature) electron-collisional plasmas suffice, as encapsulated in the famous Burgess (1965) General Formula.

2.3.2. Photoionized plasmas. These are characterized by low-temperatures, and densities. If the ground term has no fine-structure, then this is just the classic Nussbaumer & Storey (1984) 'accidental' near threshold resonances example. Such occurrences are much more likely for the M-shell than L-shell. If the ground term has fine-structure, then entire Rydberg series can contribute. An extreme example is C^+ DR which peaks at 2K. The main requirement is still for zero-density totals, but there is some interest in DR from metastable fine-structure levels — which can be quite different from the ground. Individual line emissivities produced as a result of, or enhanced by, DR can also be a useful spectral diagnostic (Nussbaumer & Storey, 1984).

2.3.3. Magnetic fusion plasmas. Here it is necessary to determine DR from both the ground and metastable states so as to treat dynamic plasmas — ones whose physical properties (temperature/density) change on the timescale of the metastable lifetimes — and to determine DR to all non-LTE final resolved states for generalized collisional–radiative modelling of density effects (e.g. stepwise ionization) and field effects (plasma microfield) — see, e.g., Summers & Hooper (1983).

2.3.4. DR Project. The Goals and Methodology are described by Badnell et al (2003). Using AUTOSTRUCTURE, extensive multi-configuration Breit–Pauli calculations of DR atomic data have been made for astrophysical and fusion relevant ions, viz., all elements up to Zn plus Kr, Mo, Xe for H-like through Mg-like isoelectronic sequences. Final-state resolved partial DR rate coefficients from the ground and metastables are archived according to the Atomic Data and Analysis Structure (ADAS) *adf09* datefile format, and are available within ADAS (Summers, 2003). Fits to zero-density totals, for initial ground and metastable levels, for ≈ 300 ions are now available online from http://amdpp.phys.strath.ac.uk/tamoc/DR . Similar data is available for RR, viz. partials in *adf48* datefile format and fits to totals from http://amdpp.phys.strath.ac.uk/tamoc/RR — see Badnell (2006c) for details. Revised electron collisional plasma coronal ionization balance (Bryans *et al* , 2006) and photoionized plasma balances (Ferland, private communication, 2007) have been computed.

3. Photoionization and opacities

3.1. Photoionization

Dielectronic recombination is the time-reversed process of photo-excitation–autoionization, while radiative recombination is the time-reversed process of direct photoionization. However, there is little overlap in the parameter space of initial and final states for plasmas not in complete thermodynamic equilibrium. Consequently, separate calculations are usually performed, with the initial and final states tailored to the application. We can, at least, use the same AUTOSTRUCTURE code and methodology to determine photoionization data required for the determination of opacities.

3.2. Opacities

Energy is produced by nuclear reactions at the centre of a star, at a temperature of a few times 10^7 K, and escapes at the stellar surface. The structure of a star is determined by the equations for conservation of mass and of energy, an equation for hydrostatic equilibrium, and by the temperature gradient. In regions for which convection does not occur, the temperature gradient is determined by the *Rosseland-mean opacity* (κ_R).

Let $\sigma_k(u)$ be the cross-section for absorption or scattering of radiation by element k, where $u = h\nu/(k_B T)$, ν is frequency and k_B is Boltzmann's constant. For a mixture of elements with number fractions f_k, $\sum_k f_k = 1$, put $\sigma(u) = \sum_k f_k \sigma_k(u)$. The Rosseland-mean cross section is

σ_{R} where,

$$\frac{1}{\sigma_{\mathrm{R}}} = \int_0^\infty \frac{F(u)}{\sigma(u)}\mathrm{d}u \tag{2}$$

and

$$F(u) = \left[\frac{15}{(4\pi^4)}\right] u^4 \exp(-u)/[1 - \exp(-u)]^2. \tag{3}$$

The Rosseland-mean opacity per unit mass is $\kappa_{\mathrm{R}} = \sigma_{\mathrm{R}}/\mu$ where μ is mean molecular weight.

The original opacities of the Opacity Project (OP) team, led by Mike Seaton, were applicable to stellar envelopes (densities, $\rho \lesssim 0.01$ g/cm^3) — see Seaton *et al* (1994). They were determined in response to the suggestion by Simon (1982) that increased opacities might explain discrepancies between theory and observations for pulsational properties of stars. At the same time, Iglesias & Rogers (1996) at Lawrence Livermore National Laboratory also produced new opacities (OPAL). OPAL and OP opacities are in good agreement at stellar temperatures and densities applicable for pulsation studies, and are a factor of about 3 larger than those in previous use. However, at the higher temperatures and densities found in deeper layers of stellar interiors, OP and OPAL opacities differ (by up to about 30%). Iglesias and Rogers (1995) suggested that this could be due to the omission by OP of important inner-shell transitions. (Basically, the excited state populations become significant, but OP only considered photoionization of the outer-shell electron and not of the core.)

Subsequently, Badnell & Seaton (2003) confirmed that these discrepancies with OPAL were due to the omission of important inner-shell transitions. Seaton & Badnell (2004) carried-out a detailed comparison between updated OP and OPAL opacities for the case of the 6-element mix (H, He, C, O, S, Fe) of Iglesias & Rogers (1995). Such data for all cosmically abundant elements (He, C, N, O, Ne, Na, Mg, Al, Si, S, Ar, Ca, Cr, Mn, Fe and Ni) were then generated by Badnell *et al* (2005). All of the inner-shell photoionization processes, both direct and resonant, were computed perturbatively with AUTOSTRUCTURE, unlike the original OP work which made use of the R-matrix method — the latter being too computationally demanding for the inner-shell work. We look at some of these results and comment-on some of the outstanding application issues.

3.3. Comparisons between OP and OPAL

We use the variable $R = \rho/T_6^3$ introduced in the OPAL work, where ρ is mass–density and $T_6 = 10^{-6} \times T$, with T in K. Figure 2 shows $\log(\kappa_{\mathrm{R}})$ against $\log(T)$ for $\log(R) = -1, -2, -3, -4$ and -6, from both OP and OPAL, for the S92 solar mix of elements of Anders & Grevesse (1989). The over-all agreement is seen to be good. The feature at $\log(T) \simeq 5.2$, usually known as the 'Z-bump', is mainly due to transitions in iron ions with $N = 13$ to 18. It is seen that, compared to OPAL, the OP feature is shifted to slightly higher temperatures. Use of the logarithmic scale for $\log(\kappa_{\mathrm{R}})$, as in figure 2, does not allow one to see the finer details of the level of agreement between the two calculations. The general level of agreement is actually in the region of 5 to 10%. An excursion to larger differences at $\log(T) \simeq 5.5$, approaching 30% at $\log(R) = -4.5$, is found in the high-temperature wing of the Z-bump, as shown on figure 2. Differences for an iron-rich mixture are more noticeable though — see Seaton & Badnell (2004).

3.4. Solar radiative interior

Helioseismology provides remarkably accurate values for the depth, R_{CZ}, of the solar convection zone (CZ). With the earlier estimates of solar element abundances (Anders & Grevesse, 1989) values of R_{CZ} and other data from helioseismology were found to be in good agreement with results from solar models computed using OPAL opacities. With recent downward revisions in metal abundances (Asplund *et al* , 2004) it is found necessary to increase opacities in the
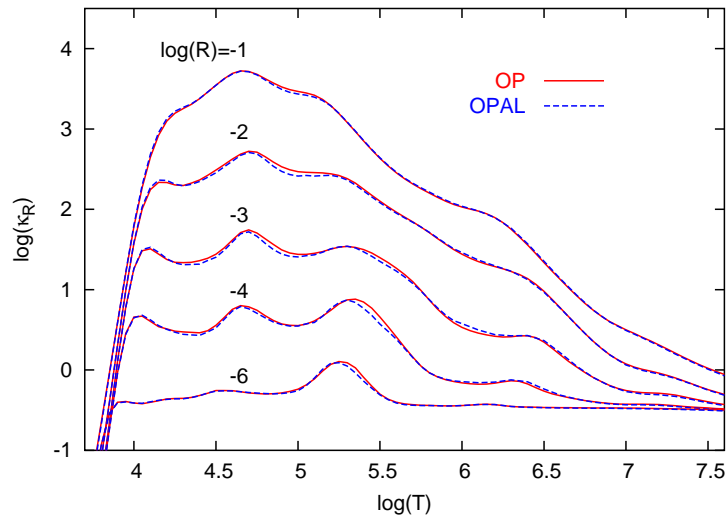
Figure 2. Rosseland-mean opacities from OP solid (red) curves and OPAL dashed (blue) curves for the S92 mix (see text), Badnell *et al* (2005). (Colour online.)

vicinity of R_{CZ}, by 19% according to Basu & Antia (2004) and by 21% according to Bahcall *et al* (2004a). Furthermore, Bahcall *et al* (2005) show that there are also discrepancies for the solar profiles of sound speed and density and of helium abundance. They argue that all such discrepancies would be removed if the opacities were larger than those from OPAL by about 10% in the region of $2 \times 10^6 \mathrm{K} \leq T \leq 5 \times 10^6 \mathrm{K}$ (0.7 to $0.4 R_{sun}$). However, the differences between OP and OPAL are much too small, as it turns out, at most 2.5%.

The problem could be solved by increasing the Ne/O abundance ratio (0.15 ± 0.03) by a factor of ~ 3. (Along with increasing other metal abundances by small amounts, i.e., within their known uncertainties.) Drake & Testa (2005) determined such an increase in Ne abundance (Ne/O≈ 0.52) from analyzing the atmospheric X-ray spectra of nearby solar-like stars. However, Young (2005) used the CDS on the SOHO satellite to observe EUV lines in Ne and O (in the quiet Sun) and used emission measure analysis to determine a Ne/O ratio of 0.17 ± 0.05, in good agreement with the 'accepted' value. Caveat: observations in stellar atmospheres are not necessarily representative of the photosphere.

3.5. Asteroseismology — gravity-mode pulsations
The Z-bump opacity (due to the Fe group, but mainly Fe and Ni) drives oscillations in low-mass B stars. Of interest is the (5000K) discrepancy between the predicted and observed high-temperature limit of the instability strip for g-mode oscillations in subdwarf B stars. The OP Z-bump occurs at a higher temperature than OPAL and it significantly affects the position of the instability strip, largely eliminating the discrepancy (Jeffery & Saio, 2006). Ni is actually key. Its opacity contribution peaks at a higher temperature than Fe and so is a more efficient absorber at the temperatures of interest.

4. R-matrix electron-impact excitation
The R-matrix method, and associated computer codes, has been used for the determination of collision data, especially electron-impact excitation, for over 30 years. It is only in the last few years that the total cross section problem for hydrogen can be considered solved within the R-matrix approach by the advent of pseudo-state methods (RMPS). This illustrates the demanding nature of the electron-collision problem. As such, it is still largely the case that one
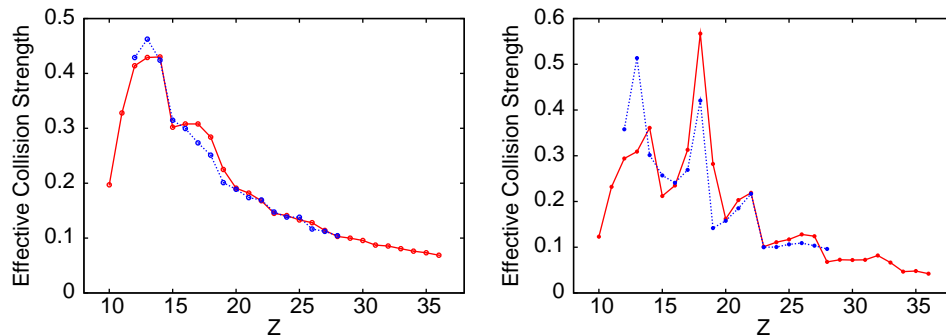
Figure 3. Electron-impact excitation of the fine-structure transition in the F-like sequence. Solid (red) curves: ICFT R-matrix, Witthoeft *et al* (2007); dashed (blue) curves: LS+JAJOM R-matrix, Berrington et al (1998). At $T = 10^4 z^2$ K (left) and $T = 10^3 z^2$ K (right). Z denotes the nuclear charge and z the residual. (Colour online.)

ion is considered at a time and the results published after a (or several) years work. To some extent now, the size of the calculation expands to fill the computer resources available. Yet the demands by modellers show no signs of abating. To fill the demand, simpler approaches such as distorted-wave, or even plane-wave Born, are often used. But, the R-matrix approach is highly useful for the production of data for modelling since it incorporates the significant, important, contribution from resonances at root. This means that population modelling need not include autoionizing levels explicitly, in general, since their main effect is incorporated in the resonant enhanced atomic data (R-matrix excitation, AUTOSTRUCTURE DR etc.). With an order of magnitude increase in computer power, even from small parallel clusters, over serial machines, it is now possible to step-back from state-of-the-art single-ion per year(s) calculations and consider, still significant, calculations along an isoelectronic sequence, at least for K- and L-shell ions, and which span most elements of astrophysical and magnetic fusion interest. There is another side to the problem — the weakness of humans. An R-matrix calculation is historically labour intensive, viz., preparation and checking of input datasets, verifying the integrity of the calculation at each 'stage', analyzing and comparing and delivering data to the user (not always in the form desired by the user). The robustness of the UK RmaX codes (http://amdpp.phys.strath.ac.uk/UK_RmaX) and the streamlining of their operation has been taken a step further with the development of an expert (Perl) script which manages every step of the calculation from the initial atomic structure determination through to the final deliverable file of Maxwell-averaged effective collision strengths, radiative rates and energy levels (in the ADAS *adf04* format) to enable a self-contained level population calculation to be performed for the ion. And, it is easily repeatable along the sequence. Hand-in-hand with this is the development of a comprehensive set of interactive Python-based GUI analysis tools to handle and verify the data produced. This approach has been implemented and applied to the F-like sequence by Witthoeft *et al* (2007) for 195CC (close-coupling) level intermediate coupling frame transformation (ICFT) calculations for all ions from Ne^+ through to Kr^{27+}. (Obviously, results for Ne^+ and other near neutral ions cannot be considered the last word, given the omission of pseudo-states, but they are better than the results of simpler methods, which would be resorted to elsewise).

We illustrate with a comparison, for the fine-structure transition, with the results of Saraph & Tully (1994) and Berrington *et al* (1998), who carried-out 2 term (from $2s^2 2p^5, 2s 2p^6$) and 28 term (plus $2s^2 2p^4 3l$) LS+JAJOM R-matrix calculations, respectively. The irregular behaviour of dis/agreement at the lower temperature considered is due to 'the march of the resonances' across threshold. At higher temperatures, the agreement is much smoother.

Future work will concentrate on further sequences around the K- and L-shell boundaries.

References

Anders E & Grevesse N 1989 *Geochim. Cosmochim. Acta.* **53** 197
Arnaud M & Raymond J 1992 *Astrophys. J.* **398** 394
Asplund M, Grevesse N, Sauval A J *et al* 2004 *Astron. Astrophys.* **417** 751
Badnell N R 1987 *J. Phys. B: At. Mol. Phys.* **19** 3827
Badnell N R 2006a *J. Phys. B: At. Mol. Opt. Phys.* **39** 4825
Badnell N R 2006b *Astrophys. J. Suppl. Ser.* **167** 334
Badnell N R 2006c *Astrophys. J. Lett.* **651** L73
Badnell N R, Bautista M A, Butler K *et al* 2005 *Mon. Not. R. astr. Soc.* **360** 459
Badnell N R, O'Mullane M G, Summers H P *et al* 2003 *Astron. Astrophys.* **406** 1151
Badnell N R & Pindzola M S 1992 *Phys. Rev.* A **45** 2820
Badnell N R & Seaton M J 2003 *J. Phys. B: At. Mol. Opt. Phys.* **36** 4367
Bahcall J N, Basu S, Pinsonneault M & Serenelli A M 2005 *Astrophys. J.* **618** 1049
Bahcall J N, Serenelli A M & Pinsonneault M 2004 *Astrophys. J.* **614** 464
Basu S & Antia H M 2004 *Astrophys. J.* **606** L85
Behar E, Jacobs V L, Oreg J *et al* 2000 *Phys. Rev.* A **62** R030501(4)
Behar E, Sako M & Kahn S M 2001 *Astrophys. J.* **563** 497
Berrington K A, Saraph H & Tully J A 1998 *Astron. Astrophys. Suppl. Ser.* **129** 161
Burgess A 1964 *Astrophys. J.* **139** 776
Burgess A 1965 *Astrophys. J.* **141** 1588
Bryans P, Badnell N R, Gorczyca T W *et al* 2006 *Astrophys. J. Suppl. Ser.* **167** 343
Drake J J & Testa P 2005 *Nature* **436** 525
Hahn Y 1989 *J. Quant. Spectrosc. Radiat. Transfer* **41** 315
Iglesias C A & Rogers F J 1995 *Astrophys. J.* **443** 469
Iglesias C A & Rogers F J 1996 *Astrophys. J.* **464** 943
Jacobs V L, Davis J, Kepple P C & Blaha M 1977 *Astrophys. J.* **211** 605–11
Jeffery C S & Saio H 2006 *Mon. Not. R. astr. Soc.* **372** L48
Kallman T & Bautista M 2001 *Astrophys. J. Suppl. Ser.* **133** 221
Kraemer S B, Ferland G J & Gabel J R 2004 *Astrophys. J.* **604** 556–61
Massey H S W & Bates D R 1942–3 *Rep. Prog. Phys.* **9** 62
Mazzotta P, Mazzitelli G, Colafrancesco S & Vittorio N 1998 *Astron. Astrophys. Suppl. Ser.* **133** 403
Netzer H 2004 *Astrophys. J.* **604** 551
Netzer H, Kaspi S, Behar E *et al* 2003 *Astrophys. J.* **599** 933
Nussbaumer H & Storey P J 1984 *Astron. Astrophys. Suppl. Ser.* **56** 293
Pindzola M S, Badnell N R & Griffin D C 1992 *Phys. Rev.* A **46** 5725
Sako M, Kahn S M & Behar E *et al* 2001 *Astron. Astrophys.* **365** L168
Saraph H & Tully J A *Astron. Astrophys. Suppl. Ser.* **107** 29
Savin D W, Gwinner G, Grieser M *et al* 2006 *Astrophys. J.* **642** 1275
Seaton M J 1962 *The Observatory* **82** 111
Schmidt E W, Schippers S, Müller A *et al* 2006 *Astrophys. J. Lett.* **641** L157
Seaton M J & Badnell N R 2004 *Mon. Not. R. astr. Soc.* **354** 457
Seaton M J, Yu Yan, Mihalas D & Pradhan A K 1994 *Mon. Not. R. astr. Soc.* **266** 805
Simon N R 1982 *Astrophys. J.* **260** L87
Summers H P 2003 *ADAS User Manual (Version 2.6)* http://adas.phys.strath.ac.uk
Summers H P & Hooper M B 1983 *Plasma Physics* **25** 1311
Witthoeft M C, Whiteford A D & Badnell N R 2007 *J. Phys. B: At. Mol. Opt. Phys.* **40** 2969
Young P 2005 *Astron. Astrophys.* **444** L45